Ore Geology Reviews 63 (2014) 1–8

Contents lists available at ScienceDirect

Ore Geology Reviews

journal homepage: www.elsevier.com/locate/oregeorev

Origin of hydrothermal deposits related to the Emeishan magmatism

Yingkui Xu [a,b], Zhilong Huang [a], Dan Zhu [a,*], Taiyi Luo [a]

[a] State Key Laboratory of Ore Deposit Geochemistry, Institute of Geochemistry, The Chinese Academy of Sciences, Guiyang 550002, China
[b] University of the Chinese Academy of Sciences, Beijing 100040, China

ARTICLE INFO

Article history:
Received 26 November 2013
Received in revised form 31 March 2014
Accepted 14 April 2014
Available online 25 April 2014

Keywords:
Hydrothermal ore deposit
Pb–Zn deposit
Underplated Emeishan basalts
Thermal simulation
Volatile
Ore-forming fluid
Sediment-hosted Pb–Zn deposits
Age of ore deposit

ABSTRACT

In the western Yangtze Block, southwest China, there are many hydrothermal native copper ore deposits and Zn–Pb ore deposits. All of these hydrothermal ore deposits are spatially associated with the Permian Emeishan flood basalts (EFBs), although they are much younger than the EFB. The maximum time interval between the hydrothermal ore deposits and the EFB is over 100 Ma. During this time interval, there is no documented magmatism in this region, and many studies indicate that magmatic fluids played important roles in the formations of these deposits. Thus, the origin of these hydrothermal deposits has long been controversial. In this study, we present a model that considers the underplated Emeishan basalts at the base of the crust as the main source of the ore-forming metals and fluids and present thermal simulation results of the evolution of the underplated Emeishan basalt. The results indicate that the underplated basalts begin to release metal-bearing fluid at 30 Ma after the onset of the underplating, consistent with age data of the oldest hydrothermal deposits in this region, such as the Huize Pb–Zn and native Cu ore deposits. The simulation results also indicate that the releasing ore-forming fluid from the crystallising underplated basalts can last over 100 Ma, which almost covers the entire age data available for the hydrothermal deposits, and thus successfully demonstrates the lack of temporal association between the hydrothermal deposits and the EFB. The model is developed primarily for the origin of the hydrothermal mineralisation in the SYG province, but it has general applicability to other sediment-hosted Pb–Zn deposits around the world.

1. Introduction

In the western Yangtze Block (Fig. 1), southwest China, there are many hydrothermal native copper ore deposits (Bing-Quan et al., 2007) and Zn–Pb ore deposits (Liu and Lin, 1999), including the world-class Huize Zn–Pb deposit with 7 million tons (Mt) of Pb and Zn metals (Han et al., 2007; Huang et al., 2004). These Zn–Pb ore deposits, which form the important Sichuan–Yunnan–Guizhou (SYG) Pb–Zn metallogenic province, contain total Pb and Zn metals of more than 20 Mt at grades of >15% Pb + Zn and have been the major source of base metals in China in the past several decades (Cromie et al., 1996; Liu and Lin, 1999). These native copper and Zn–Pb ore deposits are spatially associated with the Permian Emeishan flood basalts (EFBs) (Fig. 1), and stable isotope studies indicate that magmatic-hydrothermal fluids were involved in the ore-forming processes, as for the native copper ore deposits (Li et al., 2004) and the Zn–Pb deposits (Huang et al., 2004; Zhou et al., 2013b). This has led many workers to suggest that the EFB was an important source of the ore-forming metals and fluids (Bing-Quan et al., 2007; Han et al., 2007; Huang et al., 2004, 2010). However, the Pb–Zn and native copper deposits (132–228 Ma) (Bing-Quan et al., 2007; Li et al., 2007; Zhou et al., 2013c) in the SYG province are much younger than the Permian EFB (259–263 Ma) (He et al., 2007; Zhou et al., 2002) (Table 1). The maximum time interval is over 100 Ma, and during this time interval, there is no documented magmatism in this region (Huang et al., 2004). Thus, the origin of this ore system in the SYG province remains controversial.

In this study, we present a model that considers the underplated Emeishan basalts at the base of the crust as the main source of the ore-forming metals and fluids and present thermal simulation results of the evolution of the underplated Emeishan basalt. The results indicate that the underplated basalts would eventually release metal-bearing fluid after several tens of millions of years and thus successfully interpret the lack of temporal association between the hydrothermal deposits and the EFB. The model is developed primarily for the origin of the hydrothermal mineralisation in the SYG province, but it has general applicability to other regions, such as the Keweenawan native copper deposit in Michigan (Bornhorst et al., 1988; Davis and Paces, 1990) and the giant Broken Hill Pb–Zn deposit (Crawford and Maas, 2009).

2. Geology of the hydrothermal deposits in the SYG province

The Pb–Zn and native copper deposits in the SYG province have an intimately spatial association with the Permian Emeishan flood basalts (Bing-Quan et al., 2007; Han et al., 2007; Huang et al., 2004) (Fig. 1B). The total maximum thickness of basaltic flows is ~5 km located in the

* Corresponding author at: State Key Lab of Ore Deposit Geochemistry, Institute of Geochemistry, Chinese Academy of Sciences, Guanshui Road, 46, Guiyang, 550002, China. Tel.: +86 0851 5891249.
E-mail address: zhudan@vip.gyig.ac.cn (D. Zhu).

http://dx.doi.org/10.1016/j.oregeorev.2014.04.010
0169-1368/

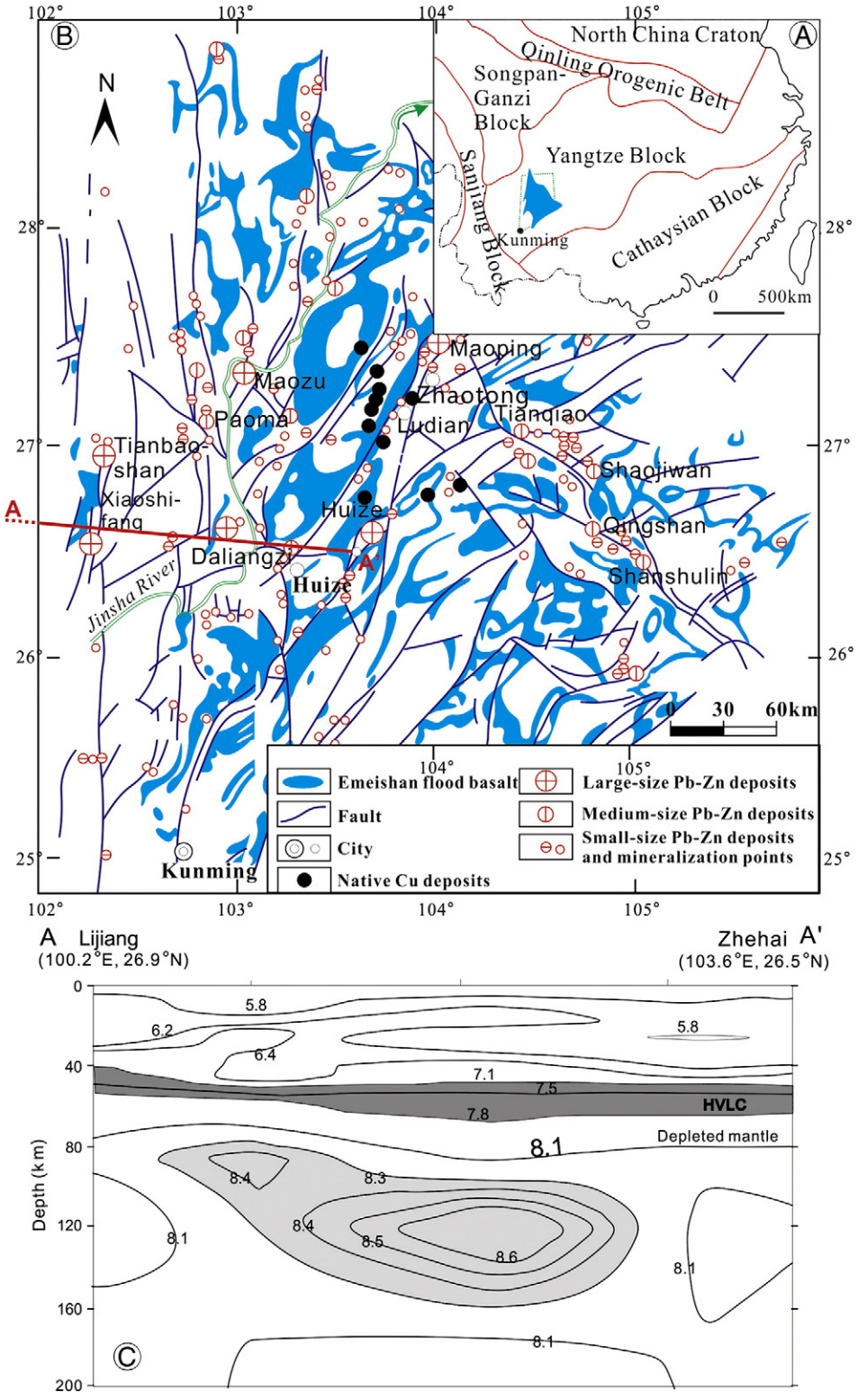

Fig. 1. Regional geological and geophysical maps. Panel A: Tectonic geological sketch; panel B: Regional geological map of the SYG Pb–Zn and native Cu metallogenic province, SW China, showing the distribution of the Permian Emeishan flood basalts, Pb–Zn and native Cu deposits, modified from Bing-Quan et al. (2007) and Huang et al. (2010)). Panel C: The seismic tomographic velocity structure of the crust and upper mantle beneath the ELIP, modified from Liu et al. (2001). The location of the seismic profile from Lijiang to Zhehai (line A–A′) is shown in panel B. HVLC — high-velocity lower crust.

western portion (i.e. Yunnan) of the Emeishan large igneous province (ELIP), whereas in the eastern portion (i.e. Guizhou) total flow thickness is only a few hundred metres (Pirajno, 2013; Shellnutt, 2013; Xu et al., 2001). The EFB is overlain by the Upper Permian Xuanwei Formation, a terrestrial coal-bearing clastic sequence (including silicalite, conglomerate, sandstone and coal beds), and is underlain by the Early Permian Maokou Formation, which consists of carbonates. The overlying Lower Triassic Feixianguan Formation consists of terrestrial sandstones and

Table 1
Ages of the EFB, Pb–Zn and native copper deposits.

	Age (Ma)	Method	Reference
Emeishan mafic intrusions	259 ± 3	Zircon U–Pb	Zhou et al. (2002)
Emeishan silicic ignimbrite	263 ± 4	Zircon U–Pb	He et al. (2007)
Native copper deposits (first stage)	226–228	$^{40}Ar/^{39}Ar$	Bing-Quan et al. (2007)
Native copper deposits (second stage)	132.2–202.2	$^{40}Ar/^{39}Ar$	Bing-Quan et al. (2007)
Huize Pb–Zn deposit	222 ± 14	Sm–Nd	Li et al. (2007)
Jinsachang Pb–Zn deposit	200	Rb–Sr	Changqing et al. (2005)
Paoma Pb–Zn deposit	200.1 ± 4	Rb–Sr	Lin et al. (2010) and Zhiyong et al. (2010)
Tianqiao Pb–Zn deposit	191.9 ± 6.9	Rb–Sr	Zhou et al. (2013c)
Maozu	196 ± 13	Sm–Nd	Zhou et al. (2013a)

shales that were deposited in small basins. The Pb–Zn deposits are hosted in the late Sinian, Devonian, Carboniferous and early Permian carbonate rocks (Huang et al., 2004), whereas the native copper deposits are restricted to a transitional zone between the uppermost part of the EFB and the Xuanwei Formation (Bing-Quan et al., 2007).

3. Magmatic fluids emitted from the underplated Emeishan basalt

Basaltic underplating is a common feature in large igneous provinces (LIP) and rifts (Ridley and Richards, 2010), such as the Emeishan LIP (Xu and He, 2007; Zhu et al., 2003). Seismic reflection and refraction reveal a heterogeneous crustal structure with a ~20 km thick high-velocity layer or bodies at the base of the crust beneath the SYG province (Liu et al., 2001) (Fig. 1C), which are generally interpreted as large igneous intrusions as a result of basaltic underplating (Zhu et al., 2003). There is a high-velocity, lens-shaped body (8.3–8.6 km/s) in the upper mantle at a depth of 110–160 km. Surrounded by a normal-velocity mantle (~8.1 km/s), this high-velocity body is ~200 km long in the east–west direction and ~50 km thick (Liu et al., 2001) (Fig. 1C). The fast mantle has been interpreted as the residue left after extensive melt extraction from the plume head (Xu and He, 2007). The location of this fast zone matches that of the thick lower crust layer.

Although the seismic tomography reflects the present-day lithosphere structure, we ascribe the generation of the thick high-velocity bodies in the lower crust and upper mantle by an Emeishan plume. The reasons for this assumption are: (1) the high-velocity lower crust is a characteristic of LIPs (Ridley and Richards, 2010); and (2) after the Emeishan magmatism, there was only minor and local Cretaceous and Cenozoic magmatism in this region (Munteanu et al., 2013), such as the alkaline ultramafic dykes (88–85 Ma) in the southwest Guizhou Province (Liu et al., 2010). Thus, we suggest that subsequent magmatisms did not significantly modify the structure of the lithosphere.

Because silicate magma always contain some small amount of dissolved H_2O (Luth, 2003), as a magma is cooled at its liquidus, the melt evolves continuously to increasingly hydrous compositions without ever encountering an invariant point that would cause it to crystallise, until it becomes a solute-rich aqueous fluid that can migrate away to leave a porous cumulate behind (Mungall and Martin, 1996). According to this model, many works have suggested that H_2O in the underplated basalts will inevitably be released to form an aqueous fluid upon complete crystallisation, and these fluids are likely Cl-rich and S-rich supercritical fluids (Kamenetsky and Kamenetsky, 2010; Newton, 2010; Newton and Manning, 2005).

With regard to the existence of fluids related to the underplated basaltic intrusions, Wannamaker et al. (2004) presented evidence from magnetotelluric sounding data that the lower crust under the Great Basin of the western US contains highly conductive, interconnected pore fluids, and they suggest that these fluids have their origin in underplated basaltic intrusions (Wannamaker et al., 2004). In addition, a well-documented example is the metamorphism in the Ivrea Zone of North Italy, for which the emitted saline solutions from the underplated basaltic magma have been assigned major roles (Franz and Harlov, 1998).

When this melt begins to release fluids depends on the compositions of the primary magmas, i.e., its initial volatile (H_2O) content, and the H_2O solubility in melts. The primary magmas supplying the Emeishan LIP are likely to be compositionally variable, reflecting different mantle sources, mantle heterogeneity, variations in melting degree and depth of melt segregation (Kamenetsky et al., 2012). Therefore, the H_2O content in the Emeishan primary magmas is also likely variable. A rough estimate of the H_2O content is the following: the bulk degree of mantle melting required to generate the Emeishan primary magma is >17% because the majority of the most fractionated basalts are not significantly depleted in platinum-group elements (Li et al., 2012) according to the classic mechanism of magmatic sulphide ore formation (Naldrett, 2012); we assume that the H_2O content in melting source is between 75 and 625 ppm., which is the range of H_2O content in the source of oceanic island basalt (Asimow and Langmuir, 2003) based primarily on the EFB being geochemically similar to the oceanic island basalt (Xu et al., 2001). Thus, the estimated H_2O content in the Emeishan primary magmas is between 0.05 and 0.4%, according to the degrees of melting (Li et al., 2012). Note that the reason that we do not consider the CO_2 here is that the behaviour of volatiles (H_2O and CO_2) during basaltic magma degassing is assumed to follow solubility laws (Dixon and Stolper, 1995; Lesne et al., 2011), which means that when volatiles degas from the silicate melt, CO_2 is exsolved deeper (and therefore earlier) than H_2O. These phenomena are well-documented (Bottinga and Javoy, 1990; Dixon and Stolper, 1995; Pichavant et al., 2013), therefore we do not need to know the CO_2 contents in the mantle source and the primary Emeishan melts.

Fig. 2 shows variations of the H_2O content during fractional crystallisation of the Emeishan primary magmas with different initial H_2O contents. The initial composition of the magma is a melt inclusion in an olivine phenocryst (Kamenetsky et al., 2012). Fractional crystallisation at 1.0 GPa total pressure and fO_2 of FMQ was simulated using the MELTS programme (Ghiorso and Sack, 1995). The H_2O

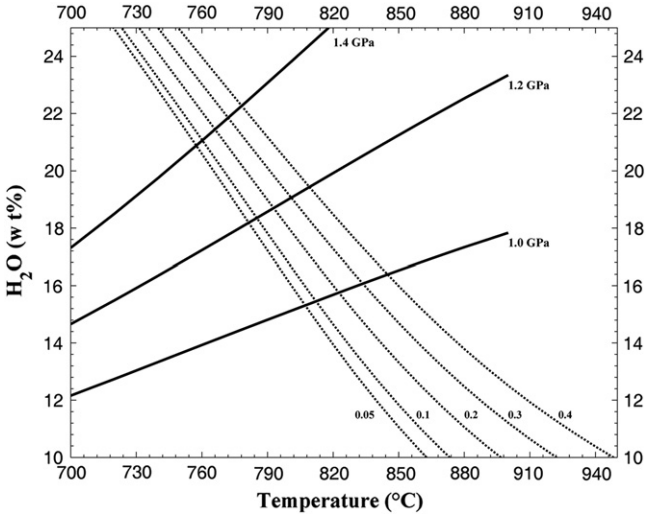

Fig. 2. Variations of the H_2O content during fractional crystallisation of Emeishan primary magmas with different initial H_2O contents (dashed lines labelled with the initial water content). The initial composition of the magma is a melt inclusion in an olivine phenocryst (M8-62) from Kamenetsky et al. (2012). Fractional crystallisation at 1.0 GPa total pressure and fO_2 of FMQ was simulated using the MELTS programme (Ghiorso and Sack, 1995). Solid dots labelled with the initial H_2O content are also shown. Solid lines (labelled with pressures) are the H_2O solubility at 1.0, 1.2 and 1.4 GPa in a rhyolitic melt (EM-34) studied by Xu et al. (2010). The H_2O solubility in a silicate melt is calculated by the Papale et al. (2006) model, which is accessible for online use at the website: http://vmsg.pi.ingv.it/index.php/en/software/interactiveArea/sw_id/4.

contents in the evolved melts increase with the degree of crystallinity, and these evolved melts are most likely interstitial melts trapped between cumulus phases as a result of the extreme differentiation (Fig. 2). The H_2O solubility at 1.0, 1.2 and 1.4 GPa in a rhyolitic melt (EM-34) studied by Xu et al. (2010), calculated by the Papale et al. (2006) model, is also shown (Fig. 2). We use the rhyolitic melt rather than the melts calculated by the MELTS programme because this rhyolitic melt represents the extreme differentiated products of the underplated Emeishan basalt (Xu et al., 2010). The interstitial melts are eventually saturated in H_2O due to the limited solubility of H_2O in silicate melts (Dixon and Stolper, 1995; Papale et al., 2006). For example, if we assume that the average initial H_2O content in the Emeishan primary magmas is 0.25%, then the average pressure of the fractional crystallisation is 1.2 GPa. When the magma cooled to 800 °C, the crystallisation is 99%, and the H_2O content in the evolved melt is 19%. Thus, this evolved melt would be saturated in H_2O and begins to release fluids (Fig. 2). In addition, the solidus of the melt is 700 °C. The reason for this is that when the total crystallisation of the underplated melts is over 99.9%, the H_2O content in the much evolved melt is over the total silicate components at this temperature (calculated by MELTS); thus, this melt can be looked at as a fluid, rather than a silicate melt. From what has been discussed above, we know that the underplated basalts begin to release fluids at 800 °C and stop at 700 °C. Therefore, we can obtain some constraints for the timing of the ore formation by simulating the thermal evolutions of the underplated Emeishan basalt.

4. Thermal simulations

We use a finite difference method to compute the thermal evolutions of the underplated Emeishan basalt. The crust domain is divided into an array of cells. A rock composition, a temperature and a melt fraction are attributed to each cell. Temperature and melt fraction are computed using the finite difference expression of the conductive equation of heat balance:

$$\rho C_p \frac{\partial T}{\partial t} + \frac{\partial X}{\partial t}\rho L = \kappa \frac{\partial^2 T}{\partial x^2} \quad (1)$$

ρ is the density, C_p is the specific heat capacity, T is the temperature, t is the time, X is the melt fraction, L is the latent heat of fusion, k is the thermal conductivity and x is the distance (vertical). The system is discretized into a one-dimensional array of cells, and Eq. (1) is solved by forward finite difference and iterative methods. The code was written with MATLAB©. The resolution of the finite difference cells is 0.5–1 km. The values of the parameters used in the model are given in Table 2. To avoid solving convection problems, the whole underplated basalts can be considered as very thin individual sills, which are distributed along the base of the crust. So the model is entirely conductive and static.

Because the magma is molten or partially molten or the lower crust would be partially melting, the solidification and partial melting will release or absorb latent heat, which must also be included (Jaupart and Mareschal, 2010). To constrain the degree of partial melting in the lower crust and the crystallisation of the intruded basalt, we assumed linear X–T relationships between T_L and T_S, where X represents the melt fraction, and T_L and T_S represent the liquidus and solidus temperature, respectively. For basalt crystallisation or partial melting of the crust:

$$X = 1 \quad T = T_L \quad (2a)$$

$$X = (T - T_S)/(T_L - T_S) \quad T_S \le T \le T_L \quad (2b)$$

$$X = 0 \quad T < T_s\,. \quad (2c)$$

Table 2
Parameters used in the thermal simulations.

Density (ρ)	Upper crust	2650 (kg m^{-3})
	Lower crust	3050
	Mantle	3300
	Underplated basalt	2830
Solidus (T_S)	Upper crust	720 (°C)
	Lower crust	820
	Mantle	1500
	Underplated basalt	700
Liquidus (T_L)	Upper crust	1200 (°C)
	Lower crust	1200
	Mantle	–
	Underplated basalt	1500
Specific heat capacity (C_p)	Upper crust	1370 (J kg^{-1})
	Lower crust	1390
	Mantle	1000
	Underplated basalt	1480
Thermal conductivity at surface temperature and pressure (κ_0)	Upper crust	3.0 (J s^{-1} m^{-1} K^{-1})
	Lower crust	2.6
	Mantle	3.5
	Underplated basalt	2.6
latent heat of fusion (L)	Upper crust	2.7×10^5 (J kg^{-1} k^{-1})
	Lower crust	3.5×10^5
	Mantle	5.5×10^5
	Underplated basalt	4.0×10^5
Thermal conductivity (κ)	$\kappa = \kappa_0(1 + 1.5 \times 10^{-3}X) / (1 + 1.0 \times 10^{-4}T)$ (J S^{-1} m^{-1} k^{-1})	

Sources: ρ, Holbrook et al. (1992) and Kay et al. (1992); C_p and L, Bohrson and Spera (2001); κ_0 and κ, Chapman and Furlong (1992); and T_S and T_L, Annen and Sparks (2002), Annen et al. (2006), and Katz et al. (2003). In the expression for thermal conductivity, z is the depth in kilometres, and T is the temperature in Kelvin.

For example, for the modelled underplated basalt, when the temperature of the underplated basalt (T) is at its liquidus (T_L) or solidus (T_S), the melt fraction (X) is 1 and 0, respectively, whereas T is between T_L and T_S, and X is calculated by Eq. (2b).

For a layer of magma brought to the base of the crust, the thermal perturbation strongly depends on the initial and boundary conditions (Jaupart and Mareschal, 2010). To obtain exact solutions, the initial and boundary conditions must be well-constrained through investigations by other disciplines. Fig. 3 shows the temperatures and pressures (depth) for the Emeishan basalt generation, calculated by the Lee et al. model (Lee et al., 2009). The average mantle potential temperature

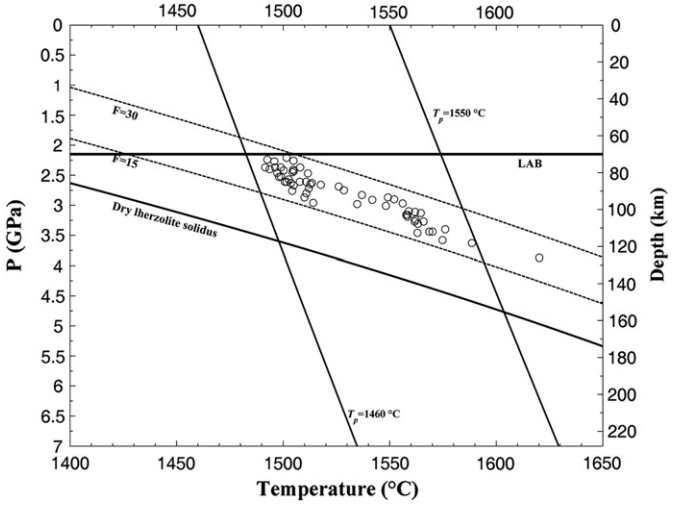

Fig. 3. Temperatures and pressures calculated by the Lee et al. model (Lee et al., 2009) for the Emeishan flood basalts (data are from the GEOROC database). Lherzolite solidus and melt fraction isopleths are from Katz et al. (2003), F = 15 and 30 represent melt fraction = 15 and 30, respectively. Near-vertical solid lines represent solid mantle adiabats.

(T_p) of the Emeishan mantle plume is 1500 °C, and the depth intervals for melt generation in the mantle are 70–130 km, which is broadly consistent with the seismic tomographic velocity structure of the upper mantle beneath the ELIP (Liu et al., 2001) (Fig. 1C). With these constraints obtained, and combined with the assumption that a normal T_p (1300 °C) is assumed at the base of the lithosphere, the initial and boundary conditions can be reasonably set (Fig. 4A).

We suggest that the onset of underplating can be looked at as the beginning of the Emeishan magmatism (259 Ma) (Zhou et al., 2002) because within 2 Ma, considerable parts of the underplated basalts cooled to less 1200 °C (see animation in the Supplementary file), part of which are believed to have erupted because they are commonly found at the surface. This indicates that the timing of the magmatic underplating and the eruption of basalts are actually identical. The simulation results show that after 30 Ma, at the onset of underplating, the uppermost part of the underplated Emeishan basalts would be cooled to 800 °C (Fig. 4B); thus, the interstitial melt was likely saturated and began to release fluids as we have previously discussed (Fig. 2). The hydrothermal deposits would begin to form, which represent the oldest hydrothermal deposits in the SYG, such as the native Cu deposits (226–228 Ma) and Huize Pb–Zn deposits (222 Ma) (Table 1). The fluids were continually released from the underplated basalts after 70 Ma because significant parts of the underplated basalts are over 700 °C (Fig. 4C), which represents the solidus of the interstitial melts, as we have discussed above. The youngest hydrothermal Pb–Zn deposits in the SYG, such as the Tianqiao Pb–Zn deposit (192 Ma), probably formed at this stage (Zhou et al., 2013c). Even after 100 Ma, the underplated basalts were able to release fluids (Fig. 4D and also see an animation in the Supplementary file); thus, it is probably representative of the second stage of native copper mineralisation at lower temperatures (100 to 200 °C) that took place during the Early Cretaceous, which is younger by over 100 Ma than the EFB, in the SYG (Bing-Quan et al., 2007).

5. Discussion and implications

There are two main factors that influence the simulation results: one is the initial H_2O content in the primary magma, and the other is the initial and boundary conditions. To evaluate factor one, we perform a test: if we assume 1% H_2O in the primary magma, this may be unrealistic in an intraplate setting. When this melt evolved to a temperature of 850 °C at a pressure of 1.2 GPa through fractional crystallisation, the H_2O content in the (interstitial) melts is 21%, calculated using MELTS, and becomes saturated in H_2O. Even in this case, the time interval is over 20 Ma between the EFB and the beginning of the degassing. This indicates that our simulation results are not sensitive to the initial H_2O content in the underplated basalts. The reason for this is that silicate

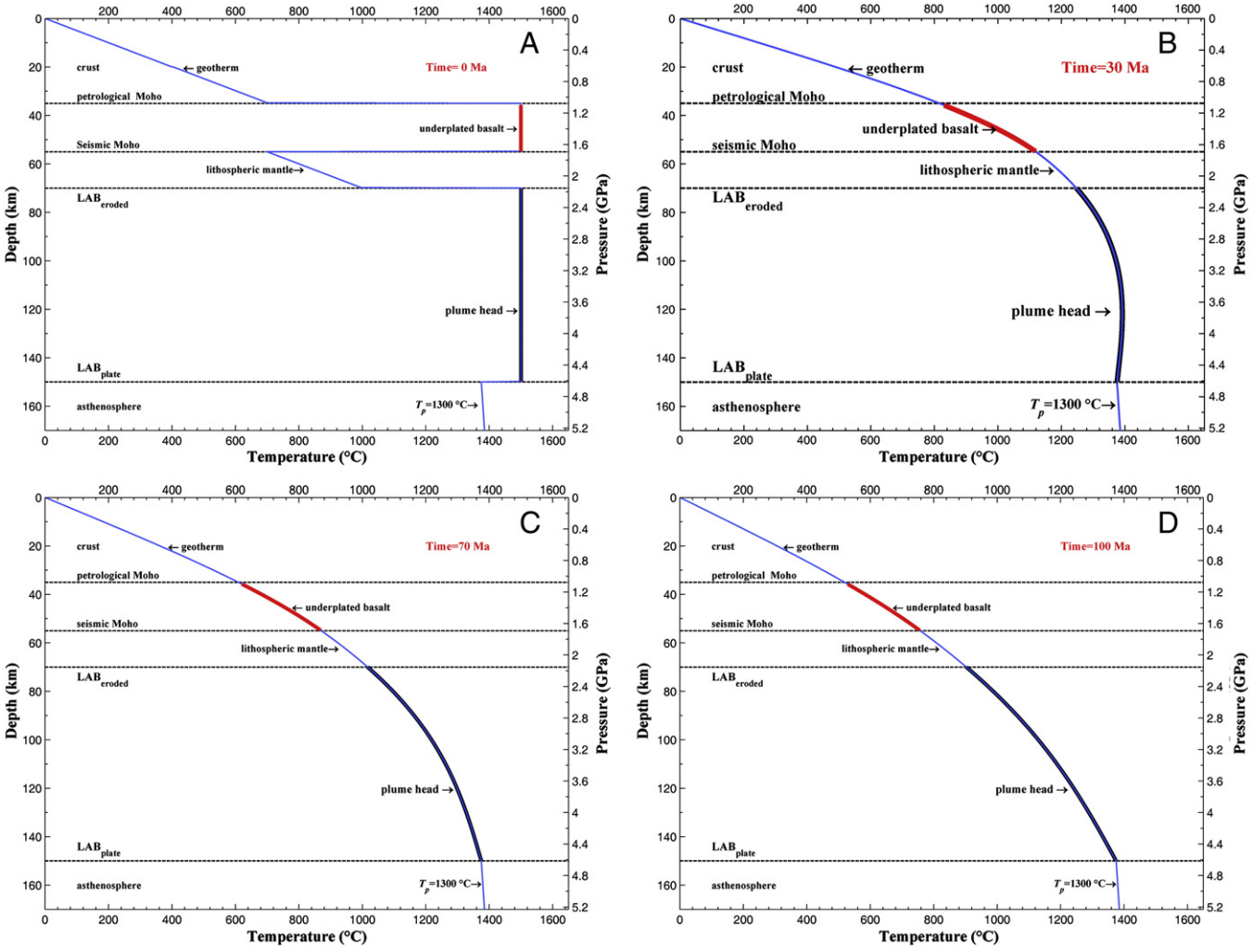

Fig. 4. Model settings and results. (A) Initial and boundary conditions; (B) the geotherm and the temperatures of the underplated Emeishan basalts after 30 Ma, 70 Ma (C) and 100 Ma (D) LAB-lithosphere–asthenosphere boundary. LAB_{plate} represents the original boundary of the lithosphere and asthenosphere before the Emeishan magmatism, whereas LAB_{eroded} represents the instantaneous boundary of the lithosphere and asthenosphere during the Emeishan magmatism.

melts have a high solubility of H_2O at high temperature (Dixon and Stolper, 1995); thus, it can effectively delay the degassing of the silicate melt.

A higher T_p with the other variables unchanged will further delay the degassing of the underplated basalt. Likewise, a previously thick crust (i.e., high pressure) has the same effect concerning the degassing of the underplated basalts due to the higher H_2O solubility in silicate melt at high pressure (Dixon and Stolper, 1995). Regarding the Emeishan basaltic underplating, because our simulation settings on the initial and boundary conditions are based primarily on the petrological and geophysical observations (Figs. 1c and 3), our simulation results may represent the real situations concerning the thermal evolutions of the underplated Emeishan basalts. Combined with the evaluation of factor one, we can safely assume that the delayed degassing of underplated basalts is a natural consequence.

In addition, using the same methods in our paper, we have simulated the thermal evolutions of Emeishan basalt sills intruded at a shallow depth (10 km) with the other variables unchanged (Fig. 5). For a 3 km thick basalt sill intruded at 10 km depth, the sill had completely solidified after 0.5 Ma; even if the basalt sill is 10 km thick, the duration for complete solidification is less than 2 Ma because the solidus of the basalt is 700 °C (Fig. 5). The results can exclude the scenario that these hydrothermal deposits formed around the roof of a pluton, and combined with the geology, the isotopic compositions and age data of the deposits further exclude the shallower origin of its metals and fluids.

The underplated Emeishan basalts as the main metal source must be verified, although the temporal links between the EFB and its hydrothermal deposits have been established by the thermal simulations. The underplated melt would likely be saturated with sulphur at a relatively early stage due to the relatively lower solubility of sulphur in silicate melts (Liu et al., 2007). Thus, immiscible sulphide liquid would be formed before fluid. According to a recent experimental results showing that chalcophile elements, such as Cu, Zn and Pb (Ag, Cd and In), can strongly partition into sulphide liquid when the FeO content in the silicate melt is extremely low (Kiseeva and Wood, 2013), then Cu, Zn and Pb would be rich in this late-stage formed sulphide liquid because the FeO content in the silicate melt has a strongly negative relation to the degree of fractional crystallisation. This Cu, Zn and Pb-rich sulphide liquid would be re-dissolved in the deuteric fluid, and the metals that had been scavenged by the sulphide liquid from the silicate melts would also go into the fluid to produce S and metal-rich ore fluid because sulphur is highly soluble in hydrous fluids (Newton and Manning, 2005). Sulphide liquid cannot survive prolonged exposure to fluid percolation. This process is similar to the formations of arc-related magmatic hydrothermal ore fluids (Nadeau et al., 2010).

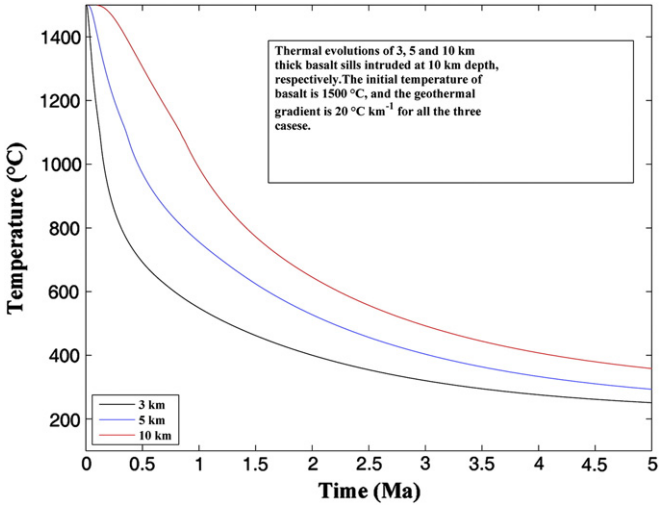

Fig. 5. Thermal evolutions of Emeishan basalt sills intruded at 10 km depth.

There is an outstanding problem of why Cu could form an independent deposit, which should be answered. We suggest that during the ascent of the supercritical fluids released from the underplated basalts, these fluids may undergo boiling as a result of depressurisation (Pirajno, 2009b). Boiling can effectively separate Cu from Pb and Zn because Cu partitions strongly into a magmatic vapour phase (Williams-Jones and Heinrich, 2005), whereas lithophile element Pb and Zn remain in the fluids. It is most likely that the Cu-rich vapour more rapidly ascends than the fluids from which it had been separated, and it then precipitated at the relatively impermeable regions, such as the zones between the flood basalts and the overlying Xuanwei Formation, to form native Cu mineralisation. If this suggestion is correct, we also predict that the lighter Cu isotope is likely rich in these native Cu mineralisations, according to recent experimental results (Rempel et al., 2012).

The recent measurement of orders of magnitude higher metal contents in fluid inclusions than previously considered allows for much smaller volumes of ore fluid to be involved in the sediment-hosted Pb–Zn mineralisation (Appold and Wenz, 2011; Wenz et al., 2012); thus, new models are needed for their formations (Wilkinson, 2014). We propose a possible genetic model for the hydrothermal deposits in the SYG. When the underplated Emeishan basalts cooled (800 °C), the interstitial melt in the cumulate was saturated in the fluid. The emitted hot fluid percolated upward through the cumulate pile and dissolved the sulphide liquid, which is rich in chalcophile elements, such as Zn, Pb and Cu, causing the percolated fluid to be rich in these chalcophile elements as well. The chalcophile element-rich fluid transported upward along the fault zones and probably underwent boiling(s) as a result of depressurisation, thus causing the formation of ore-forming vapour for native Cu mineralisation, which precipitated at the relatively impermeable regions to form the native Cu mineralisation. When the acidic hydrothermal fluid met the carbonate rocks, it would precipitate sphalerite and galena as a result of cooling and reaction with limestone or mixing with local meteoric waters to form a carbonate-hosted Pb–Zn deposit in the SYG.

The origin of hydrothermal deposits is unequivocally by precipitation from aqueous solutions within the upper several kilometres of the crust (Pirajno, 2009a). Because many sediment-hosted Pb–Zn ore deposits are characterised by the absence of temporally associated igneous rocks, the traditional thinking about the source of ore-forming metals and fluid are sedimentary and basement rocks and their related fluids (Leach et al., 2010). As we have shown in this study, the underplated basalt can provide not only metals but also fluids; thus, this novel mechanism for the formation of hydrothermal ore deposits may also work in other hydrothermal deposits in the world because many sediment-hosted Pb–Zn ore deposits are spatially associated with igneous rocks.

As we mentioned earlier, underplating is a common feature in LIPs and rifts (Ridley and Richards, 2010); thus, many hydrothermal deposits in LIPs and rifts may be related to basaltic underplating. For example, the formation of the Keweenawan native copper deposit in Michigan, which is aged between 1060 and 1047 Ma (Bornhorst et al., 1988) and is 40 Ma younger than the basaltic flows in the same region (Davis and Paces, 1990), may have a link with the basaltic underplating; and probably the giant Broken Hill Pb–Zn deposit in eastern Australia also can be formed in this way (Crawford and Maas, 2009).

Supplementary data to this article can be found online at http://dx.doi.org/10.1016/j.oregeorev.2014.04.010.

Acknowledgements

This study was supported by grants 2014CB440905, SKLODG-ZY125-06, 41072054 and 40772059. We are grateful to the official

review by three anonymous reviewers and editorial handling by the editor Prof. Franco Pirajno.

References

Annen, C., Sparks, R.S.J., 2002. Effects of repetitive emplacement of basaltic intrusions on thermal evolution and melt generation in the crust. Earth Planet. Sci. Lett. 203 (3–4), 937–955.

Annen, C., Blundy, J.D., Sparks, R.S.J., 2006. The genesis of intermediate and silicic magmas in deep crustal hot zones. J. Petrol. 47 (3), 505–539.

Appold, M.S., Wenz, Z.J., 2011. Composition of ore fluid inclusions from the Viburnum Trend, Southeast Missouri District, United States: implications for transport and precipitation mechanisms. Econ. Geol. 106 (1), 55–78.

Asimow, P.D., Langmuir, C.H., 2003. The importance of water to oceanic mantle melting regimes. Nature 421 (6925), 815–820.

Bing-Quan, Z., Yao-Guo, H., Zheng-Wei, Z., Xue-Jun, C., Tong-Mo, D., Guang-Hao, C., Jian-Hua, P., Yong-Ge, S., De-Han, L., Xiang-Yang, C., 2007. Geochemistry and geochronology of native copper mineralization related to the Emeishan flood basalts, Yunnan Province, China. Ore Geol. Rev. 32 (1–2), 366–380.

Bohrson, W.A., Spera, F.J., 2001. Energy-constrained open-system magmatic processes II: application of Energy-Constrained Assimilation-Fractional Crystallization (EC-AFC) model to magmatic systems. J. Petrol. 42 (5), 1019–1041.

Bornhorst, T.J., Paces, J.B., Grant, N.K., Obradovich, J.D., Huber, N.K., 1988. Age of native copper mineralization, Keweenaw Peninsula, Michigan. Econ. Geol. 83 (3), 619–625.

Bottinga, Y., Javoy, M., 1990. MORB degassing: bubble growth and ascent. Chem. Geol. 81 (4), 255–270.

Changqing, Z., Jingwen, M., Suoping, W., 2005. Distribution, characteristics and genesis of Mississippi Valley-type lead–zinc deposits in Sichuan–Yunnan–Guizhou area. Mineral Deposits 24 (3), 336–348 (in Chinese with English abstract).

Chapman, D.S., Furlong, K.P., 1992. Thermal state of the continental lower crust. In: Fountain, D.M., Arculus, R., Kay, R.W. (Eds.), Continental Lower Crust. Elsevier, Amsterdam, pp. 179–199.

Crawford, J.C., Maas, R., 2009. A magmatic-hydrothermal origin for the giant broken hill Pb–Zn deposit. Proceedings 10th Biennial SGA Meeting, Townsville, pp. 421–423.

Cromie, P.W., Gosse, R.R., Zhang, P., Zhu, X., 1996. Exploration for carbonate-hosted Pb–Zn deposits, Sichuan, P.R.C. Proceedings 30th International Geological Congress, Beijing, China, p. 412.

Davis, D.W., Paces, J.B., 1990. Time resolution of geologic events on the Keweenaw peninsula and implications for development of the Midcontinent rift system. Earth Planet. Sci. Lett. 97 (1–2), 54–64.

Dixon, J.E., Stolper, E.M., 1995. An experimental study of water and carbon dioxide solubilities in mid-ocean ridge basaltic liquids. Part II: applications to degassing. J. Petrol. 36 (6), 1633–1646.

Franz, L., Harlov, D.E., 1998. High-grade K-feldspar veining in granulites from the Ivrea–Verbano Zone, Northern Italy: fluid flow in the lower crust and implications for granulite facies genesis. J. Geol. 106 (4), 455–472.

Ghiorso, M.S., Sack, R.O., 1995. Chemical mass-transfer in magmatic processes IV. A revised and internally consistent thermodynamic model for the interpolation and extrapolation of liquid–solid equilibria in magmatic systems at elevated-temperatures and pressures. Contrib. Mineral. Petrol. 119 (2–3), 197–212.

Han, R.-S., Liu, C.-Q., Huang, Z.-L., Chen, J., Ma, D.-Y., Lei, L., Ma, G.-S., 2007. Geological features and origin of the Huize carbonate-hosted Zn–Pb–(Ag) District, Yunnan, South China. Ore Geol. Rev. 31 (1–4), 360–383.

He, B., Xu, Y.G., Huang, X.L., Luo, Z.Y., Shi, Y.R., Yang, Q.J., Yu, S.Y., 2007. Age and duration of the Emeishan flood volcanism, SW China: geochemistry and SHRIMP zircon U–Pb dating of silicic ignimbrites, post-volcanic Xuanwei Formation and clay tuff at the Chaotian section. Earth Planet. Sci. Lett. 255 (3–4), 306–323.

Holbrook, W.S., Mooney, W.D., Christensen, N.I., 1992. The seismic velocity structure of the deep continental crust. In: Fountain, D.M., Arculus, R., Kay, R.W. (Eds.), Continental Lower Crust. Elsevier, Amsterdam, pp. 1–43.

Huang, Z.L., Chen, J., Han, R.S., 2004. Geochemistry and Ore-formation of the Huize Giant Lead–Zinc Deposit, Yunnan, Province, China: Discussion on the Relationship between the Emeishan Flood Basalts and Lead–Zinc Mineralization. Geological Publishing House, Beijing.

Huang, Z., Li, X., Zhou, M., Li, W., Jin, Z., 2010. REE and C–O isotopic geochemistry of calcites from the world-class Huize Pb–Zn deposits, Yunnan, China: implications for the ore genesis. Acta Geol. Sin. Eng. Ed. 84 (3), 597–613.

Jaupart, C., Mareschal, J.C., 2010. Heat Generation and Transport in the Earth. Cambridge University Press.

Kamenetsky, V.S., Kamenetsky, M.B., 2010. Magmatic fluids immiscible with silicate melts. Examples from Inclusions in Phenocrysts and Glasses, and Implications for Magma Evolution and Metal Transport. Frontiers in GeofluidsWiley-Blackwell pp. 293–311.

Kamenetsky, V.S., Chung, S.L., Kamenetsky, M.B., Kuzmin, D.V., 2012. Picrites from the Emeishan Large Igneous Province, SW China: a compositional continuum in primitive magmas and their respective mantle sources. J. Petrol. 53 (10), 2095–2113.

Katz, R.F., Spiegelman, M., Langmuir, C.H., 2003. A new parameterization of hydrous mantle melting. Geochem. Geophys. Geosyst. 4 (9), 1073.

Kay, R.W., Kay, S.M., Arculus, R.J., 1992. Magma genesis and crustal processing. In: Fountain, D.M., Arculus, R., Kay, R.W. (Eds.), Continental Lower Crust. Elsevier, Amsterdam, pp. 423–445.

Kiseeva, E.S., Wood, B.J., 2013. Chalcophile element partitioning between silicate and sulphide liquids. Proceedings 23th Annual VM Goldschmidt Conference, Florence, Italy (25–30 August 2013).

Leach, D.L., Bradley, D.C., Huston, D., Pisarevsky, S.A., Taylor, R.D., Gardoll, S.J., 2010. Sediment-hosted lead–zinc deposits in Earth history. Econ. Geol. 105 (3), 593–625.

Lee, C.T.A., Luffi, P., Plank, T., Dalton, H., Leeman, W.P., 2009. Constraints on the depths and temperatures of basaltic magma generation on Earth and other terrestrial planets using new thermobarometers for mafic magmas. Earth Planet. Sci. Lett. 279 (1–2), 20–33.

Lesne, P., Kohn, S.C., Blundy, J., Witham, F., Botcharnikov, R.E., Behrens, H., 2011. Experimental simulation of closed-system degassing in the system basalt-H2O–CO^2–S–Cl. J. Petrol. 52 (9), 1737–1762.

Li, H.M., Mao, J.W., Zhang, C.Q., Xu, H., Chen, Y.C., Wang, D.H., 2004. Isotopic geochemistry of Emeishan copper deposits in northeastern Yunnan and western Guizhou. Mineral Deposits 23, 232–240 (in Chinese with English abstract).

Li, W., Huang, Z., Yin, M., 2007. Dating of the giant Huize Zn–Pb ore field of Yunnan Province, southwest China: constraints from the Sm–Nd system in hydrothermal calcite. Resour. Geol. 57 (1), 90–97.

Li, C.S., Tao, Y., Qi, L., Ripley, E.M., 2012. Controls on PGE fractionation in the Emeishan picrites and basalts: constraints from integrated lithophile–siderophile elements and Sr–Nd isotopes. Geochim. Cosmochim. Acta 90, 12–32.

Lin, Z., Wang, D., Zhang, C., 2010. Rb–Sr isotopic age of sphalerite from the Paoma lead–zinc deposit in Sichuan Province and its implications. Geol. China 37 (2), 488–494.

Liu, H.C., Lin, W.D., 1999. Study on the Law of Pb–Zn–Ag Ore Deposit in Northeast Yunnan. Yunnan University Press, Kunming.

Liu, J.H., Liu, F.T., He, J.K., Chen, H., You, Q.Y., 2001. Study of seismic tomography in Panxi paleorift area of southwestern China — structural features of crust and mantle and their evolution. Sci. China. Ser. D Earth Sci. 44 (3), 277–288.

Liu, Y., Samaha, N.-T., Baker, D.R., 2007. Sulfur concentration at sulfide saturation (SCSS) in magmatic silicate melts. Geochim. Cosmochim. Acta 71 (7), 1783–1799.

Liu, S., Su, W., Hu, R., Feng, C., Gao, S., Coulson, I.M., Wang, T., Feng, G., Tao, Y., Xia, Y., 2010. Geochronological and geochemical constraints on the petrogenesis of alkaline ultramafic dykes from southwest Guizhou Province, SW China. Lithos 114 (1–2), 253–264.

Luth, R.W., 2003. Mantle volatiles — distribution and consequences. In: Heinrich, D.H., K. K. T. (Eds.), Treatise on Geochemistry. Oxford, Pergamon, pp. 319–361.

Mungall, J.E., Martin, R.F., 1996. Extreme differentiation of peralkaline rhyolite, Terceira, Azores; a modern analogue of Strange Lake, Labrador? Can. Mineral. 34 (4), 769–777.

Munteanu, M., Yao, Y., Wilson, A.H., Chunnett, G., Luo, Y., He, H., Cioacă, M., Wen, M., 2013. Panxi region (South–West China): tectonics, magmatism and metallogenesis. A review. Tectonophysics 608, 51–71.

Nadeau, O., Williams-Jones, A.E., Stix, J., 2010. Sulphide magma as a source of metals in arc-related magmatic hydrothermal ore fluids. Nat. Geosci. 3 (7), 501–505.

Naldrett, A.J., 2012. Fundamentals of magmatic sulfide deposits. In: Li, C.S., Ripley, E.M. (Eds.), Magmatic Ni–Cu and PGE Deposits: Geology, Geochemistry, and Genesis. Reviews in Economic Geology, vol. 62, pp. 1–50.

Newton, R.C., 2010. Role of saline fluids in deep-crustal and upper-mantle metasomatism: insights from experimental studies. Geofluids 10 (1–2), 58–72.

Newton, R.C., Manning, C.E., 2005. Solubility of anhydrite, CaSO4, in NaCl–H2O solutions at high pressures and temperatures: applications to fluid–rock interaction. J. Petrol. 46 (4), 701–716.

Papale, P., Moretti, R., Barbato, D., 2006. The compositional dependence of the saturation surface of, H2O + CO2 fluids in silicate melts. Chem. Geol. 229 (1–3), 78–95.

Pichavant, M., Carlo, I., Rotolo, S., Scaillet, B., Burgisser, A., Gall, N., Martel, C., 2013. Generation of CO2-rich melts during basalt magma ascent and degassing. Contrib. Mineral. Petrol. 166 (2), 545–561.

Pirajno, F., 2009a. Metalliferous Sediments and Sedimentary Rock-hosted Stratiform and/or Stratabound Hydrothermal Mineral Systems, Hydrothermal Processes and Mineral Systems. Springer, Netherlands pp. 727–883.

Pirajno, F., 2009b. Water and Hydrothermal Fluids on Earth, Hydrothermal Processes and Mineral Systems. Springer, Netherlands pp. 1–71.

Pirajno, F., 2013. Large igneous provinces (Xiong'er, Dashigou, 827 Ma Event, Tarim, Emeishan) and the Yanshanian tectono-thermal event of eastern China. The Geology and Tectonic Settings of China's Mineral DepositsSpringer, Netherlands pp. 547–638.

Rempel, K.U., Liebscher, A., Meixner, A., Romer, R.L., Heinrich, W., 2012. An experimental study of the elemental and isotopic fractionation of copper between aqueous vapour and liquid to 450 °C and 400 bar in the CuCl–NaCl–H2O and CuCl–NaHS–NaCl–H2O systems. Geochim. Cosmochim. Acta 94, 199–216.

Ridley, V.A., Richards, M.A., 2010. Deep crustal structure beneath large igneous provinces and the petrologic evolution of flood basalts. Geochem. Geophys. Geosyst. 11 (9), Q09006.

Shellnutt, J.G., 2013. The Emeishan large igneous province: a synthesis. Geosci. Front. 5 (3), 369–394.

Wannamaker, P.E., Caldwell, T.G., Doerner, W.M., Jiracek, G.R., 2004. Fault zone fluids and seismicity in compressional and extensional environments inferred from electrical conductivity: the New Zealand Southern Alps and U.S. Great Basin. Earth Planets Space 56 (12), 1171–1176.

Wenz, Z.J., Appold, M.S., Shelton, K.L., Tesfaye, S., 2012. Geochemistry of Mississippi Valley-type mineralizing fluids of the Ozark Plateau: a regional synthesis. Am. J. Sci. 312 (1), 22–80.

Wilkinson, J.J., 2014. 13.9 — sediment-hosted zinc–lead mineralization: processes and perspectives, In: Holland, H.D., Turekian, K.K. (Eds.), Treatise on Geochemistry, 2nd ed. Elsevier, Oxford, pp. 219–249.

Williams-Jones, A.E., Heinrich, C.A., 2005. 100th Anniversary Special Paper: vapor transport of metals and the formation of magmatic-hydrothermal ore deposits. Econ. Geol. 100 (7), 1287–1312.

Xu, Y.-G., He, B., 2007. Thick, high-velocity crust in the Emeishan large igneous province, southwestern China: evidence for crustal growth by magmatic underplating or intraplating. Geological Society of America Special Papers 430, 841–858.

Xu, Y.G., Chung, S.L., Jahn, B.M., Wu, G.Y., 2001. Petrologic and geochemical constraints on the petrogenesis of Permian–Triassic Emeishan flood basalts in southwestern China. Lithos 58 (3–4), 145–168.

Xu, Y.-G., Chung, S.-L., Shao, H., He, B., 2010. Silicic magmas from the Emeishan large igneous province, Southwest China: petrogenesis and their link with the end-Guadalupian biological crisis. Lithos 119 (1–2), 47–60.

Zhiyong, L., Denghong, W., Changqing, Z., 2010. Rb–Sr isotopic age of sphalerite from the Paoma lead–zinc deposit in Sichuan Province and its implications. Geol. China 37 (2), 488–494 (in Chinese with English abstract).

Zhou, M.F., Malpas, J., Song, X.Y., Robinson, P.T., Sun, M., Kennedy, A.K., Lesher, C.M., Keays, R.R., 2002. A temporal link between the Emeishan large igneous province (SW China) and the end-Guadalupian mass extinction. Earth Planet. Sci. Lett. 196 (3–4), 113–122.

Zhou, J., Huang, Z., Yan, Z., 2013a. The origin of the Maozu carbonate-hosted Pb–Zn deposit, southwest China: constrained by C–O–S–Pb isotopic compositions and Sm–Nd isotopic age. J. Asian Earth Sci. 73, 39–47.

Zhou, J.X., Gao, J.G., Chen, D., Liu, X.K., 2013b. Ore genesis of the Tianbaoshan carbonate-hosted Pb–Zn deposit, Southwest China: geologic and isotopic (C–H–O–S–Pb) evidence. Int. Geol. Rev. 55 (10), 1300–1310.

Zhou, J.X., Huang, Z.L., Zhou, M.F., Li, X.B., Jin, Z.G., 2013c. Constraints of C–O–S–Pb isotope compositions and Rb–Sr isotopic age on the origin of the Tianqiao carbonate-hosted Pb–Zn deposit, SW China. Ore Geol. Rev. 53, 77–92.

Zhu, D., Luo, T.-Y., Gao, Z.-M., Zhu, C.-M., 2003. Differentiation of the Emeishan flood basalts at the base and throughout the crust of southwest China. Int. Geol. Rev. 45 (5), 471–477.